Friction Stir Welding of AZ31 Mg Alloy: Microstructure, Micro hardness and Electrochemical Behavior

Khawla Amara, Mabrouk Bouabdallah, Riad Badji, and Mouloud Aissani

Abstract− In this investigation, rolled plates of AZ31 Mg alloy were successfully friction-stir welded. It was found that the process leads to the microstructural refinement in the NZ due to the dynamic recrystallization with a global microstructural heterogeneity through the weld. The maximum microhardness values were attributed to the finest microstructure. The obtained results revealed that the cathodic behavior of the grain boundaries improves the corrosion resistance of the NZ. Thus, the corrosion resistance enhancement was ascribed to the most homogeneous microstructure and the finest grains.

***Keywords*− AZ31 magnesium alloy, electrochemical behavior, friction stir welding, micro-hardness, microstructure.**

NOMENCLATURE

FSW	Friction stir welding.
NZ	Nugget zone.
BM	BM.
HAZ	Heat-affected zone.
TMAZ	Thermomechanically affected zone.
IMC	Intermetallic compound.
OCP	Open circuit potential
PDP	Potentiodynamic polarization
EIS	Electrochemical impedance spectroscopy

I. INTRODUCTION

Owing to the exceptional features of lightness, specific resistance, and damping capacity, magnesium and its alloys are extensively employed throughout the automotive [1] and aerospace [2]. Even so, the conventional welding processes involving fusion reveal the poor weldability of Mg alloys with defects such as hot cracks, porosity and high residual stresses [3]. To ameliorate joint efficiency, FSW can effectively alternate the conventional welding processes and become a more efficient joining process [4],[5]. Further, numerous studies have been carried out on the microstructure, crystallographic texture, and mechanical properties of the AZ31 FSW joint [6]–[8]. The FSW microstructures are characterized by recrystallized fine grain, tiny second phases with uniform distribution, and dominance of the basal texture in the NZ [9], [10] [11]. This characterized microstructure contributes to the enhancement of the ultimate tensile strength, and microhardness, and decreases the residual stress level [8]. Besides, numerous papers reported that grain refinement of the FSW AZ31 joint significantly improves its corrosion resistance [12] whereas others denied the effect of grain boundary [13] and attributed the corrosion resistance to the cathodic Al-Mn IMCs [13], [14]. Thus, this study aims to examine the microstructure in the area that has undergone the most significant evolution NZ and TMAZ compared to the BM. The purpose of this investigation is to characterize the microstructural evolution and related electrochemical behavior in the BM, TMAZ, and NZ zones which experienced crucial microstructural changes in a friction stir welded joint of AZ31 magnesium alloy.

Manuscript received April 27, 2023; revised July 5, 2024.

K. Amara is with Ecole Nationale Polytechnique, Algiers, ALGERIA (e-mail: amara_khawla@hotmail.fr).

M. Bouabdallah was with Ecole Nationale Polytechnique, Algiers, ALGERIA(e-mail: mabrouk.bouabdallah@g.enp.edu.dz).

R. Badji is with the Research Center in Industrial Technologies, Algiers, ALGERIA (e-mail: r.badji@crti.dz)

M. Aissani is with the Research Center in Industrial Technologies, Algiers, ALGERIA (e-mail:m.aissani@ crti.dz)

Digital Object Identifier (DOI): 10.53907/enpesj.v4i1.198

II. MATERIALS AND EXPERIMENTAL PROCEDURES

The material used in this study is an 8 mm thick rolled plate of AZ31 Mg alloy with a nominal chemical composition (Mg - 2.9Al - 0.87Zn - 0.37Mn). The plates were prepared in the desired dimensions (200 x 100) mm ^{2} and friction stir welded at a rotational speed of 950 rpm and a welding speed of 43 mm/min, as described previously [15].

The joint has been cut perpendicularly to the welding direction. Microstructure observation was realized on a transversal cross-section. The samples underwent a metallographic preparation consisting of mechanical polishing followed by a finishing polishing by a diamond suspension and eventually etched with Picral reagent (4.2 g picric acid, 10 ml acetic acid, 70 ml ethanol and 10 ml distilled water). The microstructures of the BM, TMAZ, and NZ were observed using (Nikon Elipse LV100ND) optical microscope and a (ZEISS – GEMINI 300) scanning electron microscope.

The micro hardness test was performed on the Vickers hardness tester (Buehler Wilson 3500) with an applied load of 100 g force and a dwell time of 20 s. The micro hardness profile was taken at the mid-thickness of a transversal cross-section; the distance between every two points is 1 mm.

Electrochemical measurements were performed in an electrochemical cell with three electrodes: working electrodes (BM, TMAZ, and NZ with an exposure area of 0.25 cm^2), an auxiliary electrode (platinum grid) and a reference electrode (SCE Ag/AgCl), connected to AMETEK-PARSTAT 3000 potentiostat, the data were collected and managed using VersaStudio software. The working electrodes were immersed

in a 3.5 wt% NaCl solution at room temperature for 1 h to reach the open circuit potential (OCP). Electrochemical impedance spectroscopy (EIS) measurements were carried out in the frequency range from 20 kHz to 0.01 Hz and Potentiodynamic polarization (PDP) was conducted in the potential range of -250 mV to +250 mV approximately the OCP with a scan rate of 0167 $mV.s^{-1}$.

III. RESULTS

Fig. 1.a shows a typical macrographic view of the AZ31 FSW joint from a transversal cross-section. Morphological characterization by optical microscope revealed the distinction of three zones, in addition to the BM, across the joint namely: NZ, TMAZ and HAZ depicted in the center area of the joint, the width of the NZ was approximately 7 mm. Furthermore, the extent of TMAZ on the retreating side (RS) is slightly greater than that on the advancing side (AS) due to the strain accumulated in RS during friction stir welding [16]. To estimate the maximum temperature calculated during FSW, the following empirical law can be used [10]:

$$\frac{T}{Tm} = k\left(\frac{W^2}{V}.\frac{1}{10^4}\right)^{\alpha} \qquad (1)$$

Where: Tm: melting temperature of the AZ31 alloy (610°C), T: maximum temperature reached during FSW in the NZ, W: rotation speed, V: welding speed, K and α: constants can be considered 0.0442 and 0.8052 respectively.

The above equation indicates that rotational speed and welding speed are the main contributors to heat generation during the FSW process. Thus, the temperature might reach high values (about 500°C) in the NZ.

Fig. 1-b displays a twinned microstructure of the BM, it consists both of relatively coarse and fine equiaxed grains with an average grain size of 10 µm. Fig. 1-c represents the microstructure of the NZ, it is characterized by fine equiaxed grains with an average grain size of 6.4 µm. The nugget zone has undergone a grain refinement as was expected [8] due to the dynamic recrystallization, under the combined effects of the excessive heat input and the severe plastic deformation. The TMAZ, shown in Fig. 1-d, contains both coarse grains elongated in the stirring direction (i.e. material flow), and some newly recrystallized grains were found at the grain boundary because of moderate plastic deformation at a relatively low temperature that this zone has experienced partially. This result is in good accordance with the analysis of the available literature [11]. The average grain size of the TMAZ is about 13 µm. Fig. 1.e represents the microstructure of HAZ. It is characterized by its similarity to the BM with a moderate presence of the IMCs, the twins have been removed because of the elevated temperature in this zone.

Fig. 2 represents the SEM image of the BM, NZ, TMAZ, and HAZ respectively. According to the Energy-dispersive Spectroscopy (EDS) analysis, these particles correspond to Al_8Mn_5 intermetallic compounds with an average atomic ratio (Al at. % /Mn at. %) of 1.91, 1.6, 1.65, and 1.65 for BM, NZ, TMAZ, and HAZ respectively. During the FSW, these IMCs are fragmented and randomly distributed along the grain boundaries in polygonal shapes with an average particle size is about 2-4 µm. The elemental composition of Al_8Mn_5 is not affected by the temperature achieved during FSW due to its high melting temperature.

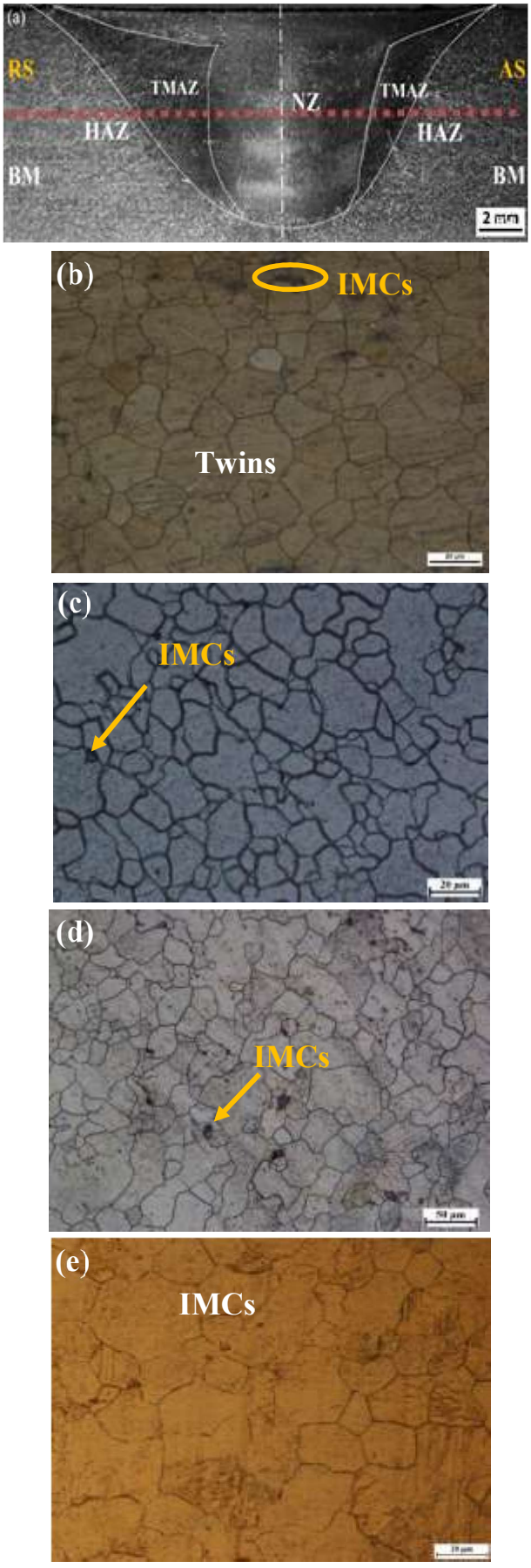

Fig. 1: Optical views of the different zones in FSW AZ31 joint (a) cross section macrostructure, (b) BM, (c) NZ, (d) TMAZ and (e) HAZ

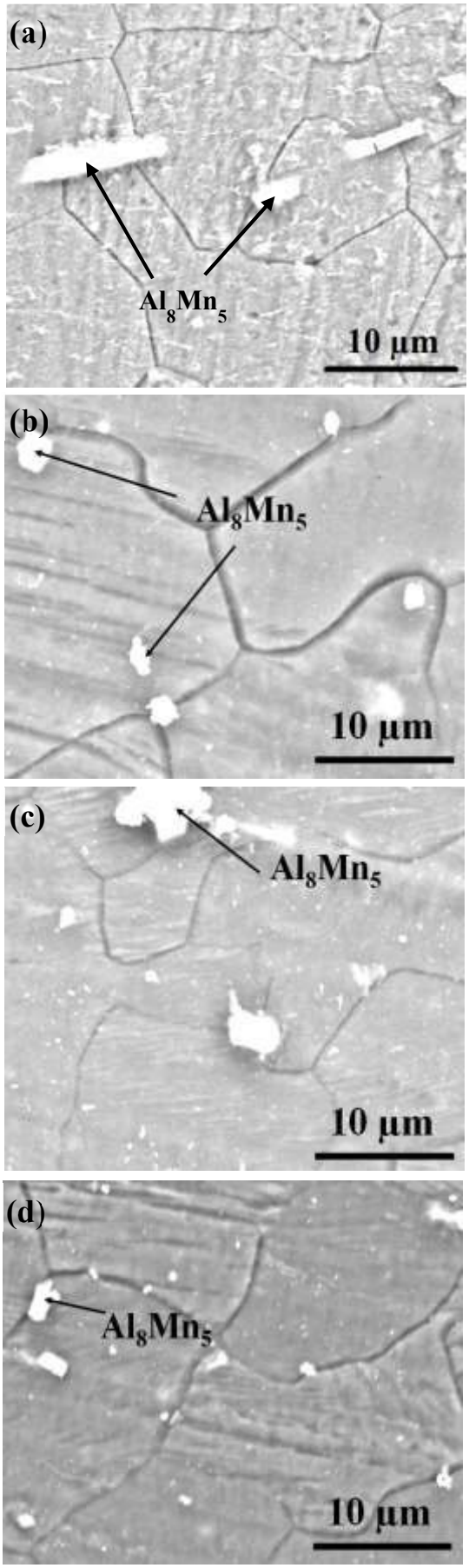

Fig. 2: SEM images of AZ31 FSW joint: (a) BM, (b) NZ, (c) TMAZ and (d) HAZ

Fig. 3 shows micro-hardness profile distribution at the midthickness of the FSW AZ31 joint. The average micro-hardness value of the BM is approximately 55 Hv.

The lowest micro hardness values were measured in HAZ at RS (~48 Hv) while the highest micro-hardness values in NZ and TMAZ were (~58 Hv). According to the Hall-Petch formula, the smaller the grain size, the higher the hardness is. The heterogeneity of the micro hardness distribution was attributed to the NZ microstructural heterogeneity. NZ underwent a high thermal input during FSW which leads to heterogeneous microstructure (fine recrystallized grains and coarse grains) while TMAZ has a higher average micro hardness compared to the other zones. This is attributed to the partial recrystallization and the high dislocation density induced by the thermo mechanical action. The presence of Al_8Mn_5 IMCs does not affect the micro hardness evolution. Such a distribution of micro hardness would be due to the unequal heat input flow and plastic deformation during FSW, which is a consequence of the heterogeneity of the microstructure.

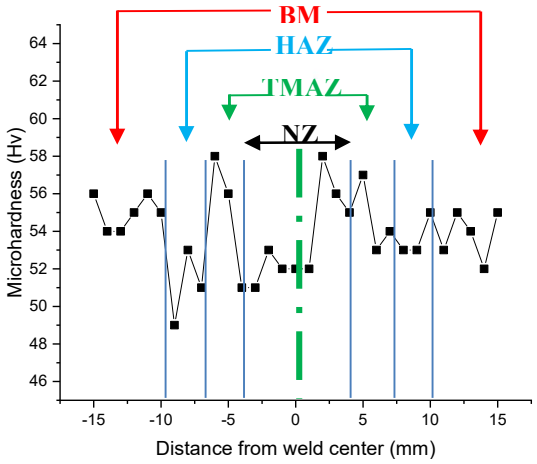

Fig. 3: Micro-hardness profile distribution of FSW AZ31 joint.

Fig. 4 and Fig. 5 summarize the electrochemical test results of BM, TMAZ, and NZ studied in a 3.5 wt% NaCl media. Fig. 4.a shows the OCP curves of the different zones of the FSW AZ31 joint. From Table I, the OCP values are classified as follows: NZ (-1.508 mV) > BM (-1.547 mV) > TMAZ (1.551 mV). Increasing the OCP value of NZ as a function of time implies the formation of a more stable oxide layer on the surface of NZ, whereas decreasing the OCP values of TMAZ and BM as a function of time may involve the destruction of the oxide layer. Thus, more positive OCP values suggest a tendency toward enhanced corrosion resistance.

Fig. 4.b displays the PDP curves of BM, TMAZ and NZ after immersion for 1 hour in 3.5 wt. NaCl. All the PDP curves present the same overall appearance, which indicates that the FSW does not affect the corrosion mechanism. These PDP curves of the NZ and TMAZ shift to the lowest current density values 17 $\mu A.cm^{-2}$ and 49 $\mu A.cm^{-2}$ respectively compared to that of the BM (52 $\mu A.cm^{-2}$). Also, the FSW seems not to affect the cathodic brunch. Nevertheless, the anodic brunch shows an inflection point corresponding to the passivity breakdown. The breakdown point Eb represents a region of intense local anodic activity that could be explained by the progressive deterioration of the oxide layer. Icorr is classified as BM<TMAZ<N. The corrosion resistance of NZ is therefore higher. This indicates that the FSW process improves the corrosion resistance of the joint regarding the BM.

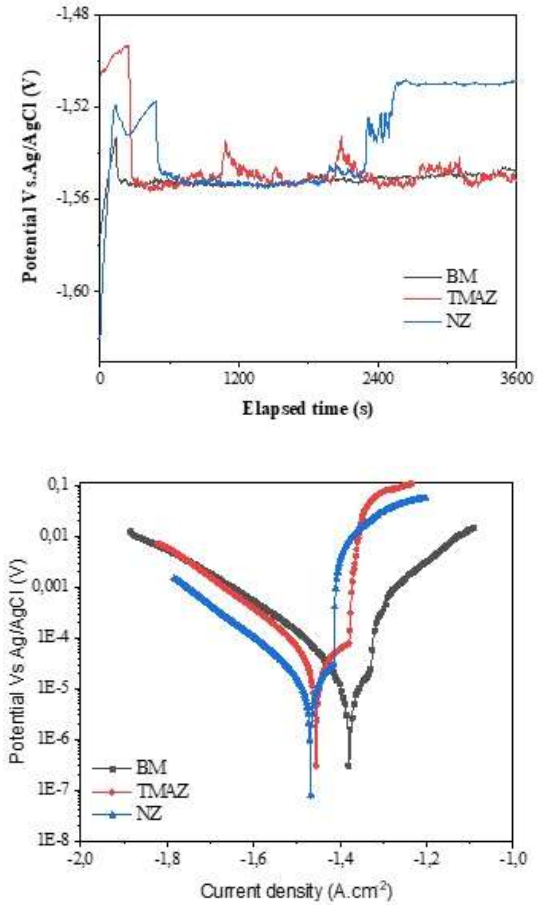

Fig. 4: Electrochemical results of the different zones in the FSW AZ31 joint in 3.5 %wt. NaCl (a) Open circuit potentiel, (b) PDP.

Table. I
POTENTIODYNAMIC POLARIZATION PARAMETERS OF THE DIFFERENT ZONES OF THE AZ31 JOINT.

	Eb (V)	*Ecorr (V)*	*Icorr (µA/cm²)*	*βc (mV)*	*βa (mV)*	*|Eb-Ecorr| (V)*	*OCP (V)*
BM	-	-1.427	52	138	-	-	-1.552
TMAZ	-1.379	-1.456	49	156	192	0.077	-1.551
NZ	-1.413	-1.468	17	160	124	0.055	-1.508

Likewise, the EIS was measured after 1 hour of immersion in 3.5 %wt. NaCl. Fig. 5.a displays the Nyquist plots of the BM, ZATM and NZ. The Nyquist plots of the BM and TMAZ consist of capacitive and inductive loops at higher and lower frequencies respectively while the Nyquist plot of the NZ consists of two capacitive loops. The loop diameter is associated with the charge-transfer resistance Rct i.e. corrosion resistance. Table II presents the Fitting parameters of Nyquist plots of the different zones in the FSW AZ31 joint in 3.5 wt% NaCl. It is concluded that the Rct values can be ranked as follows: BM (102 Ω.cm^2) < TMAZ (350 Ω.cm^2) < NZ (2093 Ω.cm^2).

The inductive loop of BM and TMAZ could be attributed to the breaking of the formed oxide layer by pitting corrosion, resulting in the dissolution of the metal in the corrosion process. The change in the inductive loop size may be indicative of a decrease in the thickness and deterioration of the oxide layer [17]. It can be suggested that the extent of the inductive loop depends on the thickness of the corrosion layer formed.

Fig 5.b and 5.c are the Bode modulus and phase respectively. The NZ shows maximum values of both Bode modulus |Z|and Bode phase, which confirms the further improvement in corrosion resistance of this zone. Furthermore, the shift in the peak position of the Bode phase confirms the deterioration of the oxide layer.

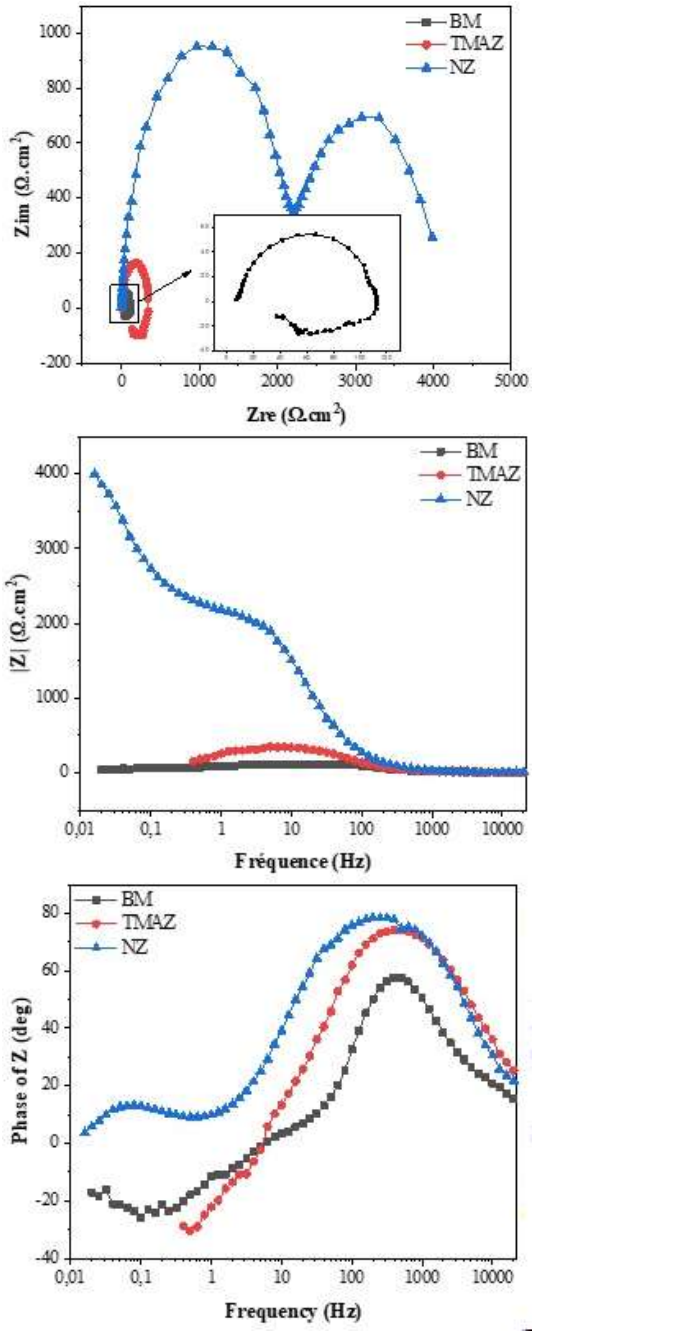

Fig. 5: electrochemical impedance spectroscopy results of the different zones in the FSW AZ31 joint in 3.5 %wt. NaCl (a) Nyquist plots, (b) Bode modulus, (c) Bode phase.

Table. II
FITTING PARAMETERS OF NYQUIST PLOTS OF THE DIFFERENT ZONES OF THE AZ31 JOINT.

	BM	***TMAZ***	***NZ***
Rs (Ω.cm²)	7.89	3.13	6.77
CPE.Y₀ (F.cm⁻² sn⁻¹)	1.53E-04	1.64E-05	9.00E-06
Freq. power n	0.9496	0.929	0.9307
C (F.cm⁻²)	1.83E-02	6.10E-04	1.06E-04
R_{ct} (Ω.cm²)	102	350	2093
CPE.Y₀ (F.cm⁻² sn⁻¹)	-	-	1.35E-03
Freq. power n	-	-	0.8926
C (F.cm⁻²)	-	-	6.09E-04
R_{ct} (Ω.cm²)	-	-	1911
Rf (Ω.cm²)	58	182	-
L (H.cm²)	75	122	-

Where Rs is the solution resistance, Rct is the resistance of the charge transfer, C is the capacitance of the oxide layer, and Rf is the resistance to the penetration of the Cl^- into the oxide layer.

IV. DISCUSSIONS

The corrosion reactions involved in neutral and alkaline environments for magnesium and their alloys are quite similar. The global reaction can be described as follows:

$$Mg + 2H_2O \rightarrow Mg(OH)_2 + H_2 \uparrow \qquad (2)$$

However, the above reaction is a general description and does not explain the involvement of the different steps of corrosion. The naturally formed oxide layer on the surface of the alloy may have high corrosion resistance. However, the same alloy may suddenly exhibit very rapid corrosion after passing a critical exposure period during which galvanic corrosion begins or after experiencing deterioration of this oxide layer. Therefore, the corrosion resistance of magnesium alloys is associated with the nature of the naturally formed oxide layer present on their surfaces and is also related to the grain boundaries and second cathodic phase present in the matrix.
The PDP curves provide the effect of the FSW on the anodic and cathodic reactions. For cathodic potential values, the Tafel curves exhibit a cathodic reaction that is characterized by hydrogen evolution as indicated by equation (3).

$$2H^+ + 2e^- \rightarrow H_2 \uparrow \qquad (3)$$

For anodic potential values, the Tafel curves exhibit an anodic reaction that is assumed to represent the anodic dissolution of α-Mg according to the reaction:

$$Mg \rightarrow Mg^{2+} + 2e^- \qquad (4)$$

The corrosion resistance of the NZ, TMAZ, and the BM, were studied and compared. It was found that after FSW, ZN exhibits higher corrosion resistance than BM and TMAZ. This is in agreement with previous work that showed that NZ is more resistant than BM [12], [19]–[21], i.e. FSW improves corrosion resistance. This is mainly attributed to grain boundaries arising from grain refinement under dynamic recrystallization in NZ (low dislocation density), those grain boundaries might act as barriers against corrosion growth due to their cathodic behavior [14], [15].
NZ owns more nucleation sites for the formation of a stable and robust oxide layer due to the high density of grain boundaries [22], [23], i.e., the grain boundaries are the most favorable sites for the nucleation of an oxide layer as the grain size decreases. As described previously in the PDP results (Table I), the passivity range on the anodic brunch confirms the formation of the oxide layer on the surface of NZ and TMAZ, which is manifested by the Eb-Ecorr difference. Therefore, it is reasonable to suggest that the enhancement in corrosion resistance may result from the increase in passivity of the oxide layer as the grain size decreases [23].

V. CONCLUSION

The effect of the FSW on the microstructure evolution and the electrochemical behavior of the BM, TMAZ, and NZ was reported in this investigation. The conclusions drawn from this study will be presented below:

- Free-defect FSW AZ31 joints were produced with heterogeneous microstructure. Al_8Mn_5 are the main IMCs with random distribution at grain boundaries.
- Irregular distribution of the micro hardness profile due to the microstructure heterogeneity with maximum values in NZ and TMAZ (58 Hv).
- The corrosion resistance depends mainly on the cathodic grain boundaries and the oxide layer formed on the surface alloy, and the difference in the corrosion rate throughout the welded joint zones was due to the microstructure heterogeneity.

REFERENCES

[1] M. K. Kulekci, « Magnesium and its alloys applications in automotive industry », Int. J. Adv. Manuf. Technol., vol. 39, no 9‑10, p. 851‑865, nov. 2008, doi: 10.1007/s00170-007-1279-2.

[2] A. H. van der Laan, R. Curran, M. J. L. van Tooren, et C. Ritchie, « Integration of friction stir welding into a multi-disciplinary aerospace design framework », Aeronaut. J., vol. 110, no 1113, p. 759‑766, nov. 2006, doi: 10.1017/S0001924000001627.

[3] F. Liu, « Microstructure, mechanical properties, and corrosion resistance of friction stir welded Mg-Al-Zn alloy thick plate joints », Weld World, p. 13.

[4] J. Zhao, F. Jiang, H. Jian, K. Wen, L. Jiang, et X. Chen, « Comparative investigation of tungsten inert gas and friction stir welding characteristics of Al–Mg–Sc alloy plates », Mater. Des., vol. 31, no 1, p. 306‑311, janv. 2010, doi: 10.1016/j.matdes.2009.06.012.

[5] S. Rajakumar, V. Balasubramanian, et A. Razalrose, « Friction stir and pulsed current gas metal arc welding of AZ61A magnesium alloy: A comparative study », Mater. Des., vol. 49, p. 267‑278, août 2013, doi: 10.1016/j.matdes.2013.01.051.

[6] W. Li, P. L. Niu, S. R. Yan, V. Patel, et Q. Wen, « Improving microstructural and tensile properties of AZ31B magnesium alloy joints by stationary shoulder friction stir welding », J. Manuf. Process., vol. 37, p. 159‑167, janv. 2019, doi: 10.1016/j.jmapro.2018.11.014.

[7] S. H. Chowdhury, D. L. Chen, S. D. Bhole, X. Cao, et P. Wanjara, « Friction Stir Welded AZ31 Magnesium Alloy: Microstructure, Texture, and Tensile Properties », Metall. Mater. Trans. A, vol. 44, no 1, p. 323336, janv. 2013, doi: 10.1007/s11661-012-1382-3.

[8] L. Commin, M. Dumont, R. Rotinat, F. Pierron, J.-E. Masse, et L. Barrallier, « Influence of the microstructural changes and induced residual stresses on tensile properties of wrought magnesium alloy friction stir welds », Mater. Sci. Eng. A, vol. 551, p. 288‑292, août 2012, doi: 10.1016/j.msea.2012.05.021.

[9] S. Mironov, T. Onuma, Y. S. Sato, et H. Kokawa, « Microstructure evolution during friction-stir welding of AZ31 magnesium alloy », Acta Mater., vol. 100, p.301‑312,nov. 2015, doi: 10.1016/j.actamat.2015.08.066.

[10] L. Commin, M. Dumont, J.-E. Masse, et L. Barrallier, « Friction stir welding of AZ31 magnesium alloy rolled sheets: Influence of processing parameters », Acta Mater., vol. 57, no 2, p. 326‑334, janv. 2009, doi: 10.1016/j.actamat.2008.09.011.

[11] J. Peng et al., « The effect of the inhomogeneous microstructure and texture on the mechanical properties of AZ31 Mg alloys processed by friction stir processing », J. Alloys Compd., vol. 792, p. 16‑24, juill. 2019, doi: 10.1016/j.jallcom.2019.04.014.

[12] F. Liu, Y. Ji, Z. Sun, J. Liu, Y. Bai, et Z. Shen, « Enhancing corrosion resistance and mechanical properties of AZ31 magnesium alloy by friction stir processing with the same speed ratio », J. Alloys Compd., vol. 829, p. 154452, juill. 2020, doi: 10.1016/j.jallcom.2020.154452.

[13] B. M. Hasani, H. Hedaiatmofidi, et A. Zarebidaki, « Effect of friction stir process on the microstructure and corrosion behavior of AZ91 Mg alloy », Mater. Chem. Phys., vol. 267, p. 124672, juill. 2021, doi: 10.1016/j.matchemphys.2021.124672.

[14] L. Lu, T. Liu, J. Chen, et Z. Wang, « Microstructure and corrosion behavior of AZ31 alloys prepared by dual directional extrusion », Mater. Des. 1980-2015, vol. 36, p. 687‑693, avr. 2012, doi: 10.1016/j.matdes.2011.12.023.

[15] K. Amara, R. Badji, M. Bouabdallah, B. Cheniti, M. Aissani, A. Haddad, A. Ziouche, « Effect of PWHT on microstructure and corrosion resistance of the nugget zone in AZ31 friction stir weld », Int J Adv Manuf Technol., vol. 123, n° 7, p. 2757–2769, dec. 2022. doi: 10.1007/s00170-022-10379-w.

[16] I. Hadji, R. Badji, M. Gaceb, et B. Cheniti, « Dissimilar FSW of AA2024 and AA7075: effect of materials positioning and tool deviation value on microstructure, global and local mechanical behavior », Int. J. Adv. Manuf. Technol., vol. 118, no 7‑8, p. 2391‑2403, févr. 2022, doi: 10.1007/s00170-021-08120-0.

[17] S. Feliu, L. Veleva, et F. García-Galvan, « Effect of Temperature on the Corrosion Behavior of Biodegradable AZ31B Magnesium Alloy in Ringer's Physiological Solution », Metals, vol. 9, no 5, p. 591, mai 2019, doi: 10.3390/met9050591.

[18] S. Feliu, L. Veleva, et F. García-Galvan, « Effect of Temperature on the Corrosion Behavior of Biodegradable AZ31B Magnesium Alloy in Ringer's Physiological Solution », Metals, vol. 9, no 5, p. 591, mai 2019, doi: 10.3390/met9050591.

[19] X. Zhang, Z. P. Cano, B. Wilson, J. R. McDermid, et J. R. Kish, « Effect of surface preparation on the corrosion resistance of friction stir linear lap welded AZ31B-H24 », Can. Metall. Q., vol. 56, no 3, p. 308–321, juill. 2017, doi: 10.1080/00084433.2017.1327500.

[20] F. Liu, Y. Ji, et Y. Bai, « Influence of multipass high rotating speed friction stir processing on microstructure evolution, corrosion behavior and mechanical properties of stirred zone on AZ31 alloy », Trans. Nonferrous Met. Soc. China, vol. 30, no 12, p. 3263–3273, déc. 2020, doi: 10.1016/S1003-6326(20)65459-0.

[21] B. Lingampalli et S. Dondapati, « Corrosion behaviour of friction stir welded ZM21 magnesium alloy », Mater. Today Proc., vol. 46, p. 1464–1469, 2021, doi: 10.1016/j.matpr.2021.03.394.

[22] D. Song, A. Ma, J. Jiang, P. Lin, D. Yang, et J. Fan, « Corrosion behavior of equal-channel-angular-pressed pure magnesium in NaCl aqueous solution », Corros. Sci., vol. 52, no 2, p. 481–490, févr. 2010, doi: 10.1016/j.corsci.2009.10.004.

[23] J. Liao, M. Hotta, et N. Yamamoto, « Corrosion behavior of fine-grained AZ31B magnesium alloy », Corros. Sci., vol. 61, p. 208–214, août 2012, doi: 10.1016/j.corsci.2012.04.039.

Khawla Amara is a Ph.D. student at the Ecole Nationale Polytechnique, Algiers, ALGERIA. She received the degree of Engineer, Master in Metallurgy from Ecole Nationale Polytechnique.

Mabrouk Bouabdallah was a Professor and research director at Ecole Nationale Polytechnique, Algiers.

Riad Badji is a Research Director at the Research Center in Industrial Technologies, Algiers.

Mouloud Aissani is a Research Director at the Research Center in Industrial Technologies, Algiers.